Tl^+-induced μs Gating of Current Indicates Instability of the MaxiK Selectivity Filter as Caused by Ion/Pore Interaction

Indra Schroeder and Ulf-Peter Hansen

Department of Structural Biology, University of Kiel, 24098 Kiel, Germany

Patch clamp experiments on single MaxiK channels expressed in HEK293 cells were performed at high temporal resolution (50-kHz filter) in asymmetrical solutions containing 0, 25, 50, or 150 mM Tl^+ on the luminal or cytosolic side with $[K^+] + [Tl^+] = 150$ mM and 150 mM K^+ on the other side. Outward current in the presence of cytosolic Tl^+ did not show fast gating behavior that was significantly different from that in the absence of Tl^+. With luminal Tl^+ and at membrane potentials more negative than −40 mV, the single-channel current showed a negative slope resistance concomitantly with a flickery block, resulting in an artificially reduced apparent single-channel current I_{app}. The analysis of the amplitude histograms by β distributions enabled the estimation of the true single-channel current and the determination of the rate constants of a simple two-state O-C Markov model for the gating in the bursts. The voltage dependence of the gating ratio $R = I_{true}/I_{app} = (k_{CO} + k_{OC})/k_{CO}$ could be described by exponential functions with different characteristic voltages above or below 50 mM Tl^+. The true single-channel current I_{true} decreased with Tl^+ concentrations up to 50 mM and stayed constant thereafter. Different models were considered. The most likely ones related the exponential increase of the gating ratio to ion depletion at the luminal side of the selectivity filter, whereas the influence of $[Tl^+]$ on the characteristic voltage of these exponential functions and of the value of I_{true} were determined by $[Tl^+]$ at the inner side of the selectivity filter or in the cavity.

INTRODUCTION

The flexibility of the selectivity filter in ion channels is still a matter of debate. After the MacKinnon group had resolved the crystal structure of KcsA (Doyle et al., 1998) the "snug fit" hypothesis of ion transport through channels seemed to be established, reinforcing the suggestion of Bezanilla and Armstrong (1972) that the "oxygens of the cage" can substitute for the water shell of the permeant ion. This concept, already anticipated by Mullins (1959), led to the postulate of a rigid structure of the selectivity filter. The rigidity was considered to be requisite for the correct distance of the carbonyl groups required for the substitution of the water shell for K^+ ions, but not for smaller Na^+ ions. Several experiments supported the snug fit hypothesis, e.g., the finding of Kiss et al. (1999) that during C-inactivation the *Shaker* K^+ channel is converted to a Na^+ channel due to the shrinkage of the tryptophane ring (Loots and Isacoff, 2000; Larsson and Elinder, 2000).

However, molecular dynamics (MD) simulations showed that a completely rigid selectivity filter cannot conduct ions (KcsA: Bernèche and Roux, 2000; Noskov and Roux, 2006, 2007). Thus, a softer picture of the channel has emerged coming closer to the field strength model of Eisenman (Eisenman, 1962; Eisenman and Horn, 1983). Here, selectivity is determined by the energy required to replace the binding of an ion to its water shell by the binding to the carbonyl groups (Varma and Rempe, 2007).

Correspondence to Ulf-Peter Hansen: uphansen@zbm.uni-kiel.de

Now, the analysis of crystal structure and MD simulations lead to a convergence of both models. Varma and Rempe (2007) found a narrow window of flexibility within which the selectivity filter achieves selective K^+ ion partitioning. The same message resulted from MD simulations of KcsA by Noskov and Roux (2006) and Noskov et al. (2004). If the filter were too rigid, K^+ ions could never physically partition from one binding site to another. If the filter were too flexible like a liquid, K^+/Na^+ selectivity could not occur. The simulations have shown that only K^+ occupies the well-ordered S0 to S4 positions in the filter. In contrast, Rb^+ (in KcsA: Morais-Cabral et al., 2001) coordinate at intermediate sites leading to different activation energies of permeation.

Most of the evidence for the flexibility comes from MD simulations, but not from experimental results. Thus, it should be investigated whether the flexibility of the filter is reflected in the gating properties of the channel. Several experiments indicate gating originating from the selectivity filter. Blunck et al. (2006) employed fluorescence measurements to prove that the inner gate of KcsA was really open when patch clamp records definitely showed gating. In GIRK channels, gating of the selectivity filter became obvious when the inner gate was locked in the open state by mutations (V188G; Yi et al., 2001).

The findings reported above lead to the question of whether the observable gating yields information about the rigidity of the selectivity filter and its interaction with the permeant ion.

J. Gen. Physiol. © The Rockefeller University Press $30.00
Volume 131 Number 4 April 2008 365–378
http://www.jgp.org/cgi/doi/10.1085/jgp.200809956

Several types of gating seem to be associated with the selectivity filter and the ions. The best-known one is C-inactivation (Kv-channels: Kurata and Fedida, 2006; Yellen, 1998; *Shaker*: Starkus et al., 1997; Choi et al., 1991; Lopez-Barneo et al., 1993), which closes the channel after prolonged depolarization. It is promoted by low K^+, and thus is also called a foot-in-the-door effect (Gibor et al., 2007). In the LQT mutant L273F of KCNQ1, two types of selectivity filter–mediated inactivation mechanism were found (Gibor et al., 2007). The fast one also occurring in WT was voltage independent and had little effect on current. It became obvious only in the tail currents. The slow one was voltage dependent. In contrast to C-inactivation, this kind of gating was promoted by elevated concentrations of external K^+. This acceleration of inactivation by external K^+ was also found in Kv2.1 (Immke et al., 1999).

The investigations here deal with fast gating, which may be similar to that found in Kir channels (Proks et al., 2001; Claydon et al., 2003; Xie et al., 2004) and may also be related to the occurrence of subconductance levels during channel opening and deactivation in the T442S mutant of *Shaker* (Zheng and Sigworth, 1998; Zheng et al., 2001). This kind of gating was considered to be related to fast structural changes in the selectivity filter. Schroeder and Hansen (2007) provided a model for the origin of the fast gating (rate constants of $10^6\ s^{-1}$) found in the negative slope in the IV curves of MaxiK at positive potentials. With increasing positive membrane potential, K^+ ions are withdrawn from the filter more rapidly than they can be refilled via the inner channel from the cytosol. This leads to ion depletion in the filter with the consequence that the ions can no longer compensate the repulsive forces of the carbonyl groups. MD simulations of Bernèche and Roux (2005) provided a suitable candidate for the molecular moiety of KcsA involved in gating. With K^+ depletion in the S2 site, the amide group between G of GYG and the neighboring V reorientates, leading to a metastable closed state. A similar picture with respect to the flipped carbonyl groups arose from molecular dynamics simulations of the mutant V127T of Kir6.2 (Capener et al., 2003).

Another approach to the relationship between ionic milieu and the stability of the selectivity filter may be provided by the flickering currents (often indicated by negative slopes in the IV curves) observed in the presence of a second monovalent cation besides K^+, like e.g., Na^+ (in MaxiK: Kawahara et al., 1990; in *Chara:* Weise and Gradmann, 2000; in KcsA: Nimigean and Miller, 2002), Cs^+ (in *Chara*: Draber and Hansen, 1994; Klieber and Gradmann, 1993), or Tl^+ (Blatz and Magleby, 1984; Farokhi et al., 2000; Ilan and Goldstein, 2001). Renart et al. (2006) have employed intrinsic tryptophane fluorescence in order to demonstrate that K^+ and Na^+ lead to different structural changes in the selectivity filter of KcsA. In the case of Tl^+ penetrating MaxiK, Piskorowski and Aldrich (2006) revealed features that are similar to those described by Schroeder and Hansen (2007). (a) The locus of interaction is in the pore since flickering in single-channel records of MaxiK channels is induced when voltage drags Tl^+ into the channel. (b) Flickering results from a destabilization of the open state. The authors argue that Tl^+ is less effective than K^+ in stabilizing the open state as indicated by the observations of Zhou and MacKinnon (2003) that only 20 mM K^+ is required to keep KcsA in the open state, but 80 mM in the case of Tl^+. Results similar to those from MaxiK were also obtained from Kir2.1 channels (Lu et al., 2001).

Here we show that the picture becomes further refined when the analysis of Tl^+-induced fast flickering in MaxiK is done with high temporal resolution as provided by the analysis of amplitude histograms by means of β distributions (Schroeder and Hansen, 2006, 2007).

MATERIALS AND METHODS

Electrophysiological Measurements

Measurements and data analysis were done along the same protocols as used by Schroeder and Hansen (2007). Patch clamp measurements were performed on inside-out patches of HEK293 cells, stably expressing an h-MaxiK α-GFP construct and the β1-subunit (Lu et al., 2006). Four different mixtures of $TlNO_3$ and KNO_3 were used with $[TlNO_3] = 0$, 25, 50, or 150 mM and $[TlNO_3] + [KNO_3] = 150$ mM. All solutions contained 2.5 mM $Ca(NO_3)_2$, 2.5 mM $Mg(NO_3)_2$, and 10 mM HEPES. The channels used here were not blocked by these concentrations of divalent cations (Schroeder and Hansen, 2007). pH was titrated with KOH to 7.2. In all experiments there was 150 mM KNO_3 on at least one side (pipette or bath) as given in the figure legends.

Patch electrodes were made from borosilicate glass (Hilgenberg) coated internally with Sigmacote (Sigma-Aldrich), drawn on a L/M-3P-A puller (Heka) and dried at 55°C overnight after pulling (Huth, 2005) in order to increase sealing probability to 100% and seal resistance to 100 GΩ. Single-channel currents under steady-state conditions were recorded by a Dagan 3900A amplifier with a 4-pole anti-aliasing filter (Bessel) of 50 kHz. Data were stored on disc with a sampling rate of 200 kHz and analyzed with the software Kiel-Patch, downhill, and Origin (see below). Liquid junction potential was not corrected, because it was <5 mV in all experiments.

Baseline drift, membrane flickering, and other artifacts would distort the amplitude histograms and lead to wrong results in the β fit. Thus, all data had to be closely inspected and cleaned manually from sections showing these kinds of artifact by means of the software Kiel-Patch. Determining apparent current amplitudes (I_{app}) by fit-by-eye using the software Kiel-Patch is described by Riessner et al. (2002).

Definitions

The definitions of states, apparent and true single-channel current have been given by Hansen et al. (2003) and Schroeder and Hansen (2007). In brief, a state lasts from t_A to t_E, if in the range (t_A, t_E) the frequency of the time intervals between the passage of two ions can be described by one asymptotic stochastic function that is independent of the length of (t_A, t_E). The true (or real) single-channel current I_{true} is the current average in such an interval (t_A, t_E). The apparent current I_{app} is the current average over a time interval that is assigned to an apparent state in a filtered

experimental record. I_{app} is identical to I_{true} if this interval is included in (t_A, t_E).

Determination of the True Current Amplitude: β Fit

The determination of I_{true} from records with fast gating by means of β distributions (FitzHugh, 1983) is described by Schroeder and Hansen (2006, 2007). Since there is no straightforward procedure to calculate β distributions obtained from higher-order filters (Riessner, 1998), simulations instead of deterministic algorithms were employed to provide the theoretical curves (Harlfinger, 2003). This is quite time consuming during a fitting routine, but it turned out to be the most efficient way to resolve fast flickering. As shown by Schroeder and Hansen (2006), it is sufficient to use a two-state Markov model (O-C) for the kinetic descriptions of the bursts in the time series. The open-point histogram (distribution-per-level, Schroeder et al., 2004) of the apparent open state (excluding the long closed states) was obtained from the time series by means of an eighth-order Hinkley detector included in the program Kiel-Patch (Schultze and Draber, 1993). For fitting the measured distribution-per-level to that one obtained from time series simulated on the basis of the two-state Markov model, a Simplex algorithm (Caceci and Caceris, 1984) was employed. Even though the fit algorithm (Schroeder and Hansen, 2006) also provides the automatic determination of the true single-channel current I_{true}, the current was used as a fixed parameter and changed stepwise in subsequent fits in order to study the dependence of the error sum on the assumed single-channel current. The inspection of this error sum curve was crucial to exclude fits that did not lead to a unique solution. The software for Kiel-Patch and for β fits (downhill) is available at www.zbm.uni-kiel.de/software.

The true single channel conductivity g_{true} was obtained from the linear range of the true single channel IV curves around 0 mV.

RESULTS

Tl^+ Effects in the ms Range

Fig. 1 presents dwell-time histograms obtained at different membrane potentials and with 150 mM K^+ or 50 mM Tl^+ + 100 mM K^+ on the luminal or on the cytosolic side. Histograms were obtained from −120 to +120 mV in steps of 20 mV, but here only the characteristic phenomena are shown. In the range of −40 to +40 mV, there is no significant influence of luminal or cytosolic Tl^+ on the dwell-time histograms of the open state (Fig. 1, C and E). A strong influence is found in the open-state histogram for luminal Tl^+ at potentials more negative than −80 mV (Fig. 1 A) and for cytosolic Tl^+ at potentials more positive than +80 mV (Fig. 1 G). This sidedness of the Tl^+ effect holds also for the closed-state histograms (Fig. 1, B, D, F, and H) with the difference that a strong effect is only observed at potentials more positive than +80 mV.

In the dwell-time histograms of Fig. 1, the lifetimes of the open states are much longer than those of the closed states as can be seen from the peaks at 1 ms in Fig. 1 A, which moves with increasing positive membrane potential to 5 ms in Fig. 1 G. The presence of Tl^+ induces an acceleration by a factor of ∼10 in Fig. 1 (A and G). The lifetimes of the closed states seem to be much faster as a clear peak is not reached at the lefthand side of the histograms. However, in the light of the analysis in the

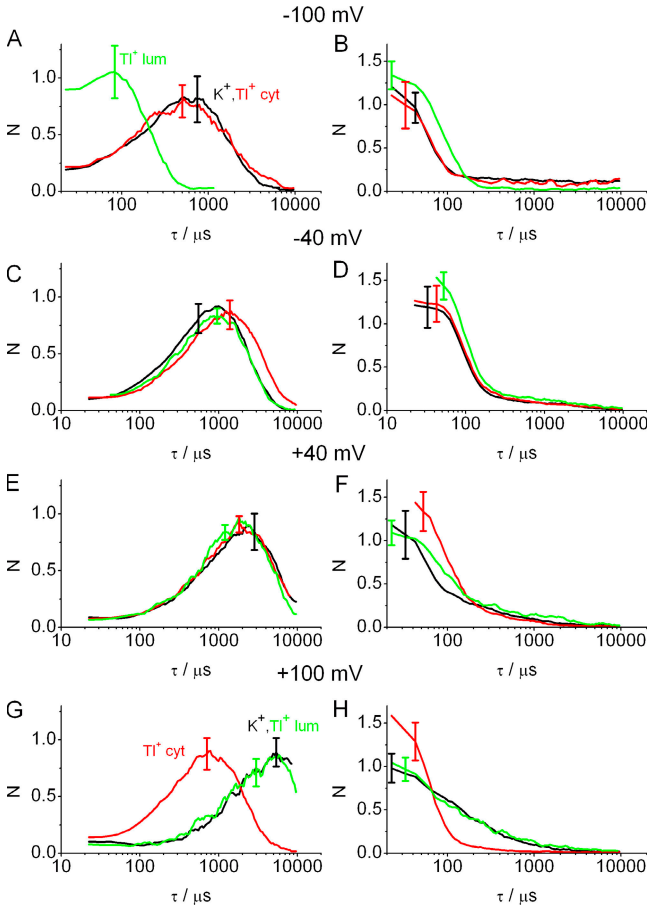

Figure 1. Dwell-time histograms of the open (A, C, E, and G) and the closed (B, D, F, and H) states obtained from MaxiK channels in the presence and absence of Tl^+ with the following solutions: 150 mM KNO_3 on both sides ('K^+', black), 50 mM Tl^+ and 100 mM K^+ on the luminal side (Tl^+ lum, green) or on the cytosolic side (Tl^+ cyt, red). On the opposite side there was always 150 mM KNO_3. 2.5 mM $Mg(NO_3)_2$ and 2.5 mM $Ca(NO_3)_2$ were included in all solutions. For the sake of clarity, only representative error bars are given, which were obtained from averaging over the error bars of bins of 25% of the τ value.

µs range described below, it seems to be likely that the open times in Fig. 1 represent the lifetimes of flickery bursts, not of a real open state. Such an analysis, however, is not an issue of the present investigation.

The results presented in Fig. 1 are very similar to those of Piskorowski and Aldrich (2006), also obtained from MaxiK (or BK) channel with a filter frequency of 20 kHz. The important common feature is the dependence of the Tl^+-induced effect on the direction of the current. The effects occur only when the electrical current drags Tl^+ into the channel. From the findings in Fig. 1 and the results of Piskorowski and Aldrich (2006) the same conclusion is drawn: the Tl^+ ions interact with the cavity and/or the selectivity filter.

Here, we refrain from a more detailed analysis of the data in Fig. 1 because of two reasons. First, a very thorough analysis has already been done by Piskorowski and

Aldrich (2006). Second, we report findings in the µs range. Thus, the only reason for displaying the data in Fig. 1 is to demonstrate that the time series of MaxiK channels investigated here show the same behavior in the ms range as those used by Piskorowski and Aldrich (2006). This emphasizes that it is the temporal range and not the usage of a different strain of MaxiK that leads to results in the µs range, which are partly very different from those obtained in the ms range.

Finding a Definition of I_{app} Being Appropriate for Model Testing

In the µs range, the gating during the often nonresolved bursts is investigated. A major issue is the distinction between I_{true} and I_{app} and the question of whether a putative molecular mechanism can provide a prediction of the measured current reduction R_I.

$$R_I = \frac{I_{true}}{I_{app}}, \tag{1}$$

as defined in Materials and methods. In flickery time series like that one in Fig. 2 A, there are two problems, i.e., determining I_{true} and an appropriate value for I_{app}. Fig. 2 illustrates the problem of estimating I_{app}. The apparent single-channel current I_{app} as obtained by fit-by-eye (horizontal lines in Fig. 2 [A and B]; Riessner et al., 2002) or from the evaluation of the amplitude histograms (vertical lines in Fig. 2, C and D) depends strongly on the integration time of the anti-aliasing filter of the recording set-up. In Fig. 2, different integration times are mimicked by the length of an offline moving average filter.

Four different definitions for the single-channel current have to be distinguished. Two of them are shown in Fig. 2, $I_{app,1}$ and $I_{app,n}$, which are obtained by a fit-by-eye (Riessner et al., 2002) from the patch clamp time series filtered by the inherent anti-aliasing filter without offline averaging ($n = 1$, Fig. 2 A) and with moving averaging over n data points (Fig. 2 B), respectively. In addition, there are the asymptotic value $I_{app,\infty}$, which is obtained with a moving average filter of sufficient length (if the burst length is long enough), and I_{true} as defined above (Hansen, 1986; Hansen et al., 2003), which can be measured directly only when gating is much slower than the corner frequency of the anti-aliasing filter.

In Fig. 3, the dependence of $I_{app,n}$ on the number of data points used in the moving average filter (n) is shown for three selected conditions that demonstrate the range of curve shapes occurring in the investigations presented here. Fig. 2 indicates that $n = 100$ is the best choice for all datasets. The graphs start at $I_{app,1}$. It has to be mentioned that $I_{app,1}$ is not I_{true}. I_{true} has to be evaluated by β fits as described by Schroeder and Hansen (2006) and as done below. The lefthand plateau does not assign a peculiar role to $I_{app,1}$, because it is nothing more than an artifact resulting from the fact that the distance between the sampling points is 5 µs and the time constant of the inherent anti-aliasing filter of 50 kHz is much longer, i.e., 20 µs.

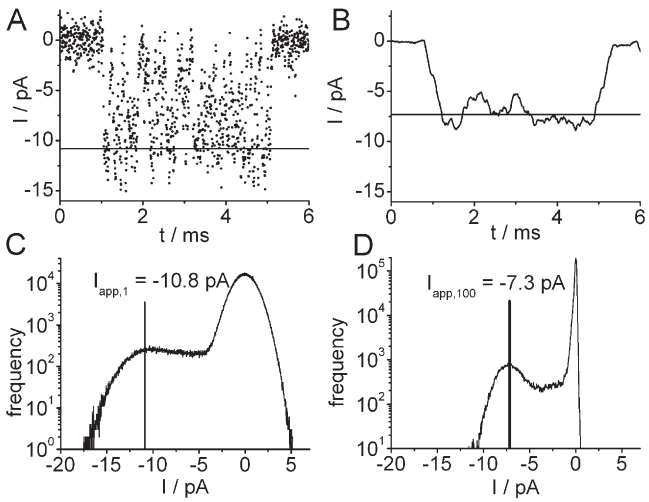

Figure 2. The effect of filtering on the apparent single-channel current. (A and C) No moving average filter (=raw data). (B and D) The same data with moving average filter over 100 data points separated by 5 µs. (A and B) The horizontal lines present I_{app} as obtained by fit-by-eye (Riessner et al., 2002). (C and D) The vertical lines present I_{app} as obtained from the maxima of the amplitude histograms of the time series above them. The time series was recorded at −120 mV with 50 mM Tl^+ + 100 mM K^+ in the pipette (luminal) and 150 mM K^+ in the bathing medium (cytosolic).

With increasing length n of the averaging interval, $I_{app,n}$ decreases until it reaches a plateau around $n = 50$–100. If the plateau is well pronounced, the current at the plateau is $I_{app,\infty}$, because here the averaging time is already long enough to reach the asymptotic value. The plateau ends when gaps between the bursts (sojourns in long-living C-states) become included in the averaging process. If a plateau is not found it is recommended to cut out all sojourns in closed states from the original time series and apply the averaging process to the remaining time series. This can be done manually by a cut routine in Kiel-Patch. In some time series (e.g., in those measured in 50 mM Tl^+), flickering is interrupted by so many sojourns into a very short closed state that cutting out of these states is nearly impossible. Then, the distributions-per-level can be generated by Kiel-Patch (Schroeder et al., 2004), and $I_{app,\infty}$ is obtained from the expectance of the current.

In the case of the data from solutions with K^+ as the sole monovalent cation (squares in Fig. 3), the difference between $I_{app,1}$ and $I_{app,\infty}$ is only 3%. This results from the high rate constants at high positive voltages, making this kind of gating so fast (closed times <1 µs, Schroeder and Hansen, 2007) that the integration time of 20 µs of the inherent anti-aliasing filter is already long enough to reach $I_{app,\infty}$ without additional offline filtering.

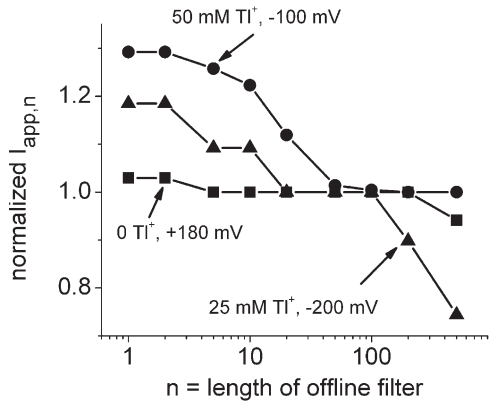

Figure 3. Dependence of $I_{app,n}$ on the number n of data points included in offline averaging. Results from three representative time series are shown.

However, Tl^+-induced gating at negative voltages is slower. The curves in Fig. 3 make obvious that now the problem arises of which value of the curves in Fig. 3 is to be used to represent the apparent current. This becomes of crucial importance when measured data are to be compared with the predictions of a putative model of the underlying molecular mechanism.

Here, it is recommended to use the current value of the plateau in Fig. 3. Of course, by means of a convolution of I_{true} with the anti-aliasing filter and the averaging process, the model could provide $I_{app,n}$ for each value of n. However, extracting the gating behavior from a putative molecular model of the channel already is complicated enough. Thus, it would not be wise to introduce further complications by involving convolution integrals. This caveat holds for $I_{app,n}$ (including $n = 1$) unless n reaches the plateau in Fig. 3. However, the value of $I_{app,\infty}$ as obtained from the plateau should be equal to $I_{app,k}$, which can easily be calculated from the model parameters by means of Eq. 3, below.

Negative Slopes and Tl^+-induced Gating

Sample recordings at −100 mV for four different concentrations of luminal Tl^+ are shown in Fig. 4. At constant membrane potential, an increase in Tl^+ concentration causes an increase in open-channel noise and a decrease in apparent single-channel current. The analysis here deals only with the bursts.

From records like those in Fig. 4, IV curves of $I_{app,\infty}$ were evaluated. In most cases, a moving average over 100 data points resulted in the asymptotic value $I_{app,\infty}$, as indicated by the plateaus in Fig. 3. However, in the case of some data obtained at 50 mM Tl^+, the expectance of the distribution-per-level had to be used instead. In the time series at the 25 mM Tl^+, the sojourns into the additional closed state interrupting the bursts were long enough to be excluded. At 150 mM Tl^+, they were so short and rare that they did not spoil the determination of the bursts. However in the 50 mM data, they were so frequent and so short that a manual elimination of the related sections was no longer possible because it became difficult to distinguish them from the bursts. The jump detector of the program Kiel-Patch (Hinkley detector, Schultze and Draber, 1993) did a more reliable job than the human eye in eliminating these short sojourns in the additional closed state when generating the distributions-per-level of the bursts.

The resulting IV curves are shown in Fig. 5 A. At positive membrane potentials where current is solely carried

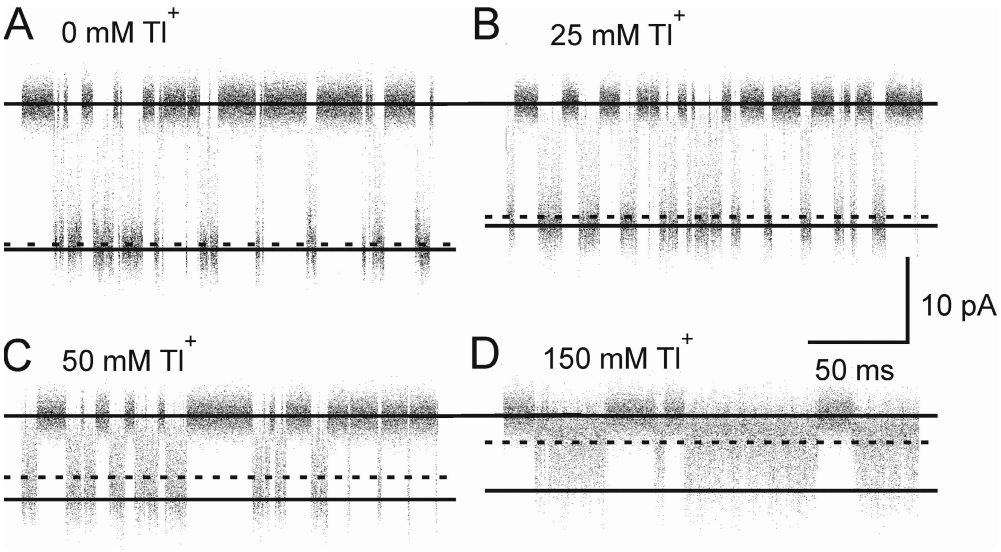

Figure 4. Sections of four current records with different K^+/Tl^+ mixtures on the luminal side (pipette). $[Tl^+]$ is given at the traces with $[K^+] = 150\ mM - [Tl^+]$. Cytosolic solution contained 150 mM K^+. Membrane potential was −100 mV for all records. Channel openings result in downward deflections. With increasing Tl^+ concentration, the open-channel noise increases and the apparent current decreases, indicating the increase of unresolved gating events. The upper horizontal lines give the baseline (closed channel). The dotted lines show the apparent current $I_{app,\infty}$ taken from the plateau in Fig. 3. $I_{app,1}$ obtained from fit-by-eye (Riessner et al., 2002) is presented by solid horizontal lines.

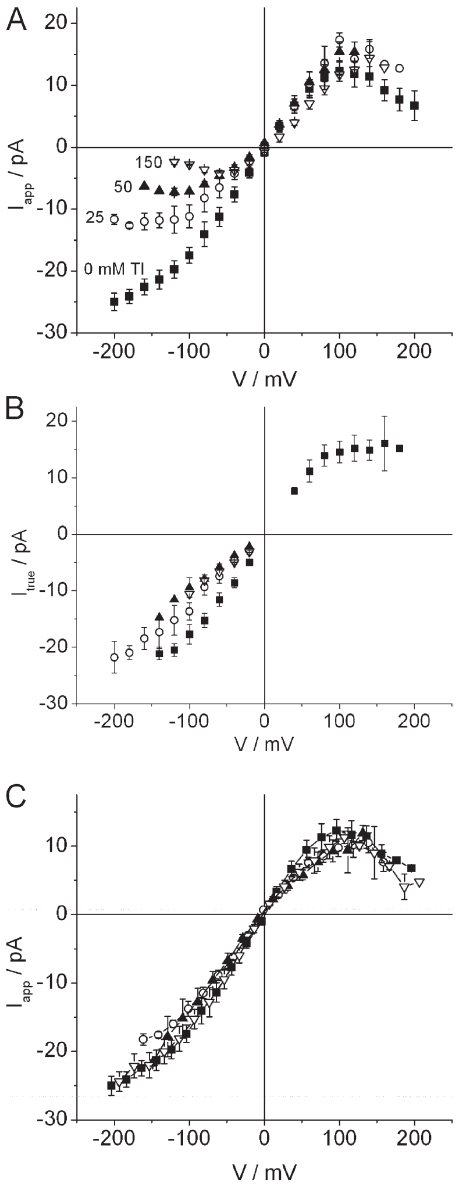

Figure 5. (A) Apparent ($I_{app,100}$) and (B) true single-channel IV curves of MaxiK with different luminal K^+/Tl^+ mixtures (pipette). The Tl^+ concentrations are attached to the curves with $[Tl^+]$ + $[K^+]$ = 150 mM. (C). Apparent IV curves obtained with cytosolic K^+/Tl^+ mixtures (bath). Besides in the region of the negative slope at positive potentials, I_{app} and I_{true} are identical.

by K^+, all IV curves show the same negative slope as the K^+ data do (Schroeder and Hansen, 2007); Tl^+ does not seem to have any significant effect. However, at negative voltages, when Tl^+ is drawn from the lumen into the pore, a second negative slope is induced. The effect increases monotonously with increasing Tl^+ concentration in the mixed solution. Similar to the negative slope on the positive side, the involvement of unresolved gating becomes obvious from the appearance of flickery current traces (Fig. 4).

The true single-channel current can be obtained from the analysis of β distributions as tested by Schroeder and Hansen (2006). The IV curves of the true single-channel current in Fig. 5 B show strong saturation at positive and a weak indication of saturation at negative membrane potentials (here, saturation is indicated by bending away from a linear IV curve). Schroeder and Hansen (2007) fitted the IV curves obtained from pure K^+ solution with a Class I model (Hansen et al., 1981). However, the related type of equation applies to many mechanisms, and thus the success of the fit does not help to select the "real" mechanism. It is just a means of a more reliable evaluation of the saturation currents. Nevertheless, there is one interesting feature in Fig. 5 B: the negative true single-channel current I_{true} in the presence of luminal Tl^+ is smaller than that in pure K^+ solution.

Fig. 5 C shows IV curves obtained with Tl^+ on the cytosolic side and K^+ as the only monovalent cation on the luminal side. There is no extra fast gating with respect to the curve obtained without Tl^+. At positive potentials, the negative slope starts even a little bit later. This may be related to the somewhat smaller conductivity in the presence of Tl^+ that was also observed in Fig. 5 B. The absence of a dramatic effect of cytosolic Tl^+ is in contrast to the findings of Piskorowski and Aldrich (2006) in MaxiK and LeMasurier et al. (2001) in KcsA and to our own results obtained from dwell-time analysis (Fig. 1). This difference results from a clear separation of fast and slow gating effects by means of the high temporal resolution employed here. Since Fig. 5 C does not yield new information with respect to the findings already published by Schroeder and Hansen (2007) for solutions without Tl^+, the following analysis only deals with the data in Fig. 5 (A and B) obtained in the presence of luminal Tl^+.

The β fit of the time series in Figs. 4 and 5 also delivers the rate constants (Fig. 6) of the two-state O-C model causing the gating in the bursts.

In Fig. 6 (A and B), rate constants are also shown for the Tl^+-free solution. In Schroeder and Hansen (2007), fast gating at negative potentials was ignored. However, the open-level distributions were slightly broader than those of the closed state, indicating the existence of a marginal current reduction by fast gating.

In the presence of luminal Tl^+, a biphasic dependence of the rate constants on Tl^+ concentration is found (Fig. 6, A and B). k_{OC} (Fig. 6 A) increases up to 50 mM Tl^+, i.e., the open state becomes less stable. Then, k_{OC} is constant above 50 mM Tl^+. The opposite trend is found in k_{CO} (Fig. 6 B). It is relatively constant at concentrations below 50 mM Tl^+ and decreases strongly above 50 mM.

The question may arise whether the opposite trends in Fig. 6 (A and B) could result from fitting artifacts. Such doubts would account for the fact that the analysis by β distributions is quite reliable in determining the ratio k_{OC}/k_{CO} (which is sufficient for the correct determination of R_k in Eq. 4a, below), but may have problems to estimate

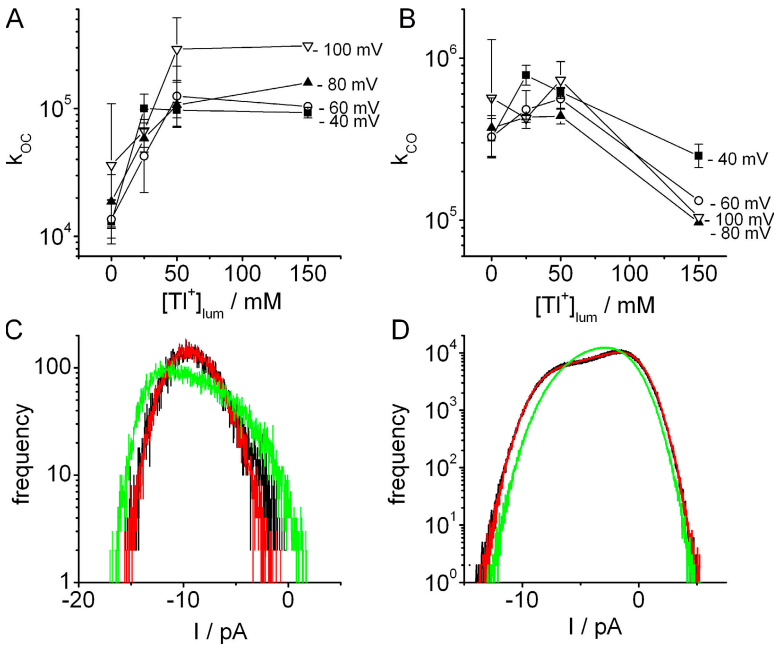

Figure 6. Dependence of the rate constants of a two-state model on luminal Tl^+ concentration at different membrane potentials as obtained from the β distributions of the current amplitudes in the bursts for (A) k_{OC} and (B) k_{CO}. C and D present tests of whether the absolute values in A and B are determined correctly. The black histograms are generated from the measured time series. The coinciding red curves result from simulated time series using the rate constants in A and B with (C) 50 mM Tl^+ at −100 mV and (D) 150 mM Tl^+ at −80 mV (a = 1 in Eq. 2). The deviating histograms (green) are obtained by multiplying the rate constants k_{CO} and k_{OC} in Eq. 2 with a common factor of (C) a = 0.33 and (D) a = 2.

the absolute values of the rate constants. With other words, the ratio

$$\frac{a\,k_{OC}}{a\,k_{CO}} = \frac{k_{OC}}{k_{CO}} \qquad (2)$$

may be determined correctly, but the common factor a may be undetermined. An adequate choice of a could shift k_{CO} at 150 mM Tl^+ upwards to give a horizontal line in Fig. 6 B and move k_{OC} at 150 Tl^+ onto the extension of the linear slope through the values at lower Tl^+ concentrations in Fig. 6 A. To exclude this objection against the results in Fig. 6 (A and B), k_{OC} and k_{CO} obtained from the fitting routine were multiplied by a common factor a (Eq. 2) and the effect on the β distributions was checked. At 150 mM, the common factor had to be 4 in order to get a horizontal line in Fig. 6 B and a monotonously increasing line in Fig. 6 A. Fig. 6 D shows that the resulting β distribution (green) differs strongly from the measured one (black) already for a factor of a = *2*. This implies that the decay in Fig. 6 B is not an artifact. Similarly, lowering k_{CO} and k_{OC} at 50 mM Tl^+ by a factor of a = *3* leads to a β distribution not representing the experimental results (Fig. 6 C). Also, the absolute values at 25 mM Tl^+ must not be changed (not depicted). Thus, the tests presented in Fig. 6 (C and D) verify the biphasic behavior shown in Fig. 6 (A and B).

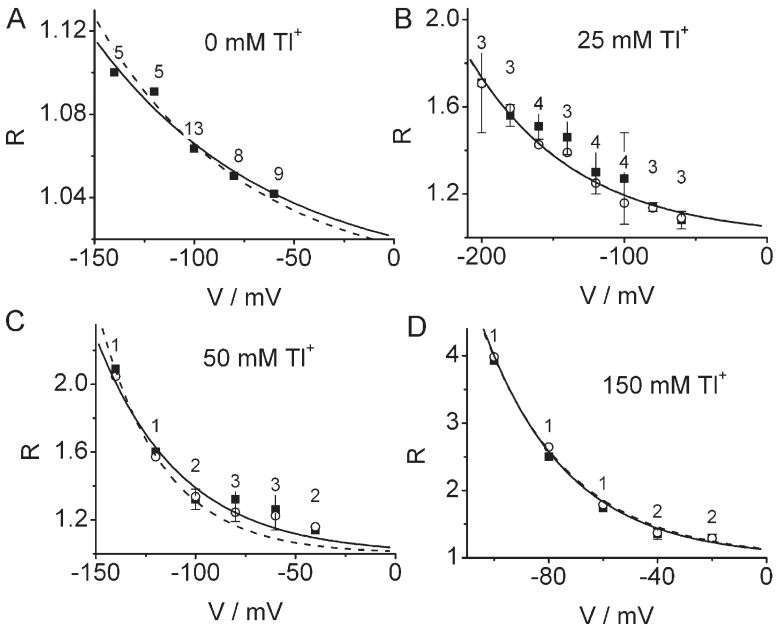

Figure 7. Dependence of the gating factor R_k (closed squares, Eq. 4a) and R_I (open circles, Eq. 4b) on membrane potential as calculated from the data in Fig. 6, A and B, and Fig. 5, A and B, respectively. The flickering bursts occurring in records at 50 mM Tl^+ were very short due to sojourns in very short closed events. There, $I_{app,\infty}$ was obtained from the expectance of current from the distributions per level (Schroeder et al., 2004). They coincided with $I_{app,k}$, indicating the high reliability of the β fit. The smooth lines present the free fits of R_k (Eq. 5, with the parameters in Table I). Dashed lines are joint fits for 0/25 mM Tl^+ and 50/150 mM Tl^+, respectively. Errors bars represent SEM. Number of data points are given at the curves.

TABLE I

Parameters of Eq. 5 as Obtained from Fitting the Voltage Dependence of the Gating Factor R in Fig. 7

	Free fit		Joint fit 0/25 and 50/150 mM	
	$R_{k,0}$	V_G /mV	$R_{k,0}$	V_G /mV
0 mM Tl^+	0.021 ± 0.009	88 ± 10	0.017 ± 0.003	76 ± 4
25 mM Tl^+	0.051 ± 0.008	72 ± 6	0.052 ± 0.007	76 ± 4
50 mM Tl^+	0.036 ± 0.012	42 ± 5	0.014 ± 0.003	32 ± 2
150 mM Tl^+	0.121 ± 0.016	31 ± 1	0.13 ± 0.02	32 ± 2

$[Tl^+]_{lum} + [K^+]_{lum} = 150$ mV.

From the rate constants in Fig. 6, $I_{app,k}$ can be calculated.

$$I_{app,k} = \frac{k_{CO}}{k_{OC} + k_{CO}} I_{true}, \tag{3}$$

with k_{CO} and k_{OC} being the rate constants of the closed–open and open–closed transitions, respectively, of the O-C two-state model employed for the β fit.

This can be used for checking whether the relationship $I_{app,\infty} = I_{app,k}$ holds and for the calculation of the gating factors R_k and R_I.

$$R_k = \frac{k_{CO} + k_{OC}}{k_{CO}} = 1 + \frac{k_{OC}}{k_{CO}} \text{ and } R_I = \frac{I_{true}}{I_{app,\infty}} \tag{4a,b}$$

In Fig. 7, R_k as calculated by Eq. 4a is compared with R_I as obtained from Eq. 4b. Both gating factors are plotted vs. membrane potential for different Tl^+ concentrations. The coincidence of R_I and R_k indicates that the relationship $I_{app,\infty} = I_{app,k}$ holds.

For 0 mM luminal Tl^+, strong gating effects occur only at positive membrane potentials as described by Schroeder and Hansen (2007). In the presence of Tl^+, the interesting gating occurs at negative potentials whereas the behavior at positive potentials is not shown as it is not different from that one found without Tl^+.

The dependence on voltage (V) of R_k at negative potentials was fitted with an exponential function as derived by Schroeder and Hansen (2007). In the Appendix the derivation of this equation was adapted for the situation here.

$$R_k = 1 + R_{k,0} \exp\left(\frac{-V}{V_G}\right) \tag{5}$$

To test whether all curves in Fig. 7 share the same characteristic voltage (as in the case of the different potassium concentrations in Schroeder and Hansen, 2007), a joint fit with shared V_G and free $R_{k,0}$ was attempted. This approach failed completely (unpublished data). However, it turned out that a reasonable joint fit with common V_G is possible for the pairs 0/25 mM Tl^+ and 50/150 mM Tl^+ (dashed lines in Fig. 7, A,B and C,D, respectively, and last columns in Table I), even though the bending was somewhat too sharp for the 0 and 50 mM data. The more likely free fit resulted in quite similar V_G for 50 and 150 mM Tl^+, but in a definitely different V_G for 0 and 25 mM Tl^+ (Table I, third column), explaining the failure of the joint fit of all concentrations. The amplitude factors $R_{k,0}$ obtained at 50 and 150 mM (Table I, second column) are proportional to the concentrations (within the scatter). This does not hold for $R_{k,0}$ obtained at 0 and 25 mM Tl^+. These numbers seem to indicate that different mechanisms are involved at 0 and 25 mM on one side and at 50 or 150 mM Tl^+ on the other side. In Fig. 8, the dependence of g_{true} of Tl^+ concentration (Fig. 8 A) is compared with the dependence of V_G (Fig. 8 B). The similar saturation behavior may lead to the suggestion that both effects result from the same mechanism. Especially, the role of 50 mM Tl^+ becomes obvious from these curves. Also the amplitude factor $R_{k,0}$ seems to change its behavior at 50 mM (Fig. 8 C) even though the scatter prevents a final statement.

DISCUSSION

The application of high temporal resolution led to results partly different from dwell-time analysis as done by Piskorowski and Aldrich (2006) and as also becomes evident from Fig. 1. Dwell-time analysis restricted to the ms range led to a symmetrical effect: Tl^+ induced a shift in the dwell times of the open and closed state when it was dragged into the channel from the cytosolic or from the luminal side. In contrast, analysis in the µs range (Figs. 5–7) revealed that Tl^+-induced gating occurred only when Tl^+ entered from the luminal side.

The fast gating effects reported here offer the chance of mechanistic explanation in terms of ion/channel interaction in the selectivity filter or the cavity as has already been suggested by Schroeder and Hansen (2007) for gating in solutions with K^+ as the only monovalent cation. Such a model has to account for the following features: (a) the exponential increase of the gating factor R with negative membrane potential; (b) the dependence of the characteristic voltage in Eq. 5 on the mole fraction Tl^+/K^+; and (c) the absence of these effects for cytosolic Tl^+.

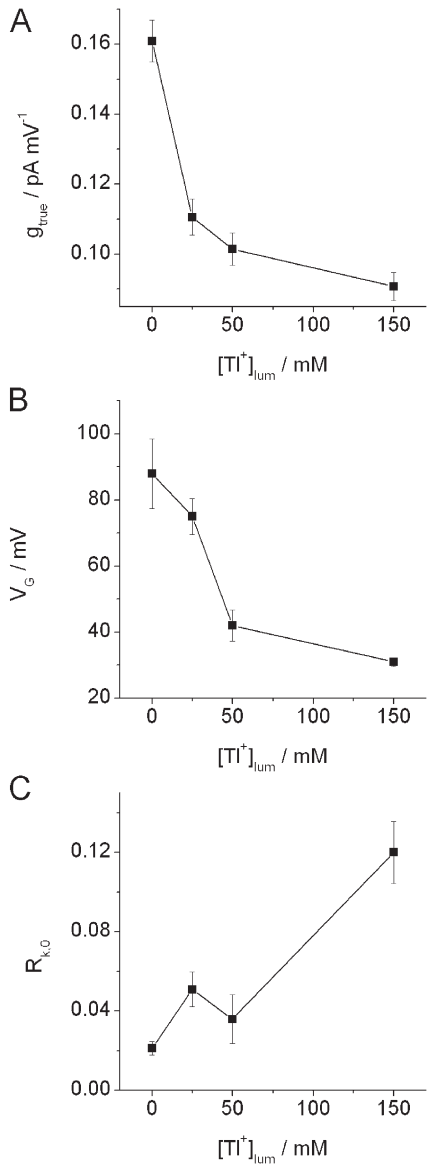

Figure 8. Dependence of (A) true single-channel conductivity g_{true} from Fig. 5 B, (B) characteristic voltage V_G (Fig. 7, Eq. 5), and (C) amplitude factor $R_{k,0}$ (Fig. 7, Eq. 5) on $[Tl^+]$ with $[Tl^+] + [K^+] = 150$ mM. Data from Table I, free fit.

In the case of fast gating found in outward currents with K^+ as the only monovalent cation, the exponential increase of the gating factor R was explained by K^+ depletion in the cavity or in the selectivity filter of MaxiK (Schroeder and Hansen, 2007). Because of the simultaneous occurrence of fast gating and saturation of the IV curves, this K^+ depletion was assumed to result from cytosolic diffusion limitation, which becomes evident when the voltage across the selectivity filter pulls ions out of the cavity or out of sites in the selectivity filter at a higher rate than that of refilling from the cytosol. The molecular mechanism that was considered as a cause of this K^+ depletion–induced gating was that found by Bernèche and Roux (2005) in molecular dynamics simulations: K^+ ions in the selectivity filter of KcsA are necessary to compensate for the repulsive forces of the carbonyl groups of the filter. K^+ depletion in the S2 site of the selectivity filter results in reorientation of the amid group between G of GYG and the neighboring V. This metastable closed state would be converted to a more stable closed state when the V-T plane, too, reorientates. Schroeder and Hansen (2007) assumed that interrupting the K^+ flux through the filter by the flickering of the metastable state keeps the average K^+ concentration at a moderate value, thus preventing the full transition into the long-lived closed state (~0.4 ms, Bernèche and Roux, 2005).

It was tempting to replace ion depletion by accumulation of unfitting ions (Tl^+) in order to adopt the hypothesis of Schroeder and Hansen (2007) to the data in Figs. 7 and 8. However, this hypothesis leads to unlikely consequences as follows. It may be suggested that at negative potentials, cytosolic diffusion limitation causes an enrichment of Tl^+ (and of K^+) in the cavity. This would be in line with the findings of Lu et al. (2001), i.e., that interaction of Tl^+ with C169 in the cavity of Kir2.1 induces structural changes that lead to a flickery state and subconductance levels (which may result from fast unresolved gating). However, an exponential increase of $[Tl^+]$ in the cavity as necessary to explain the curves in Fig. 7 is unlikely because of the limited capacity of the cavity (being occupied by nearly one ion in KcsA, Zhou and MacKinnon, 2004). Even if we ignore this objection, the situation becomes even worse: ion accumulation in the cavity would lead to an exponentially increasing inward current. This implication is in contradiction to the curvature found in Fig. 5 B, which indicates saturation at high negative potentials.

Thus, voltage-driven Tl^+ enrichment does not provide a key for the understanding of the exponential increase of the gating effects in Figs. 7 and 8. (Nevertheless, below, a slight accumulation of Tl^+ in the cavity or the internal side of the filter is considered as a secondary effect.) The exponential increase of R_k has to be mediated by a different mechanism. It may be suggested that voltage exerts a direct action on the gating properties as mediated by the S4 helix or by other voltage sensors. The viral channel Kcv (Kang et al., 2004) has no S4 helix but shows voltage-dependent gating and negative slopes in whole-cell currents, indicating the existence of a voltage sensor (Gazzarrini et al., 2002, 2006). The Kcv also produces a negative slope in single-channel measurements (Shim et al., 2007). Thus, the S4 is not the only choice for mediating a direct effect of voltage on the protein.

However, we dislike the hypothesis of a direct voltage action on gating because it employs unproven ad hoc assumptions not backed up by the data presented here. Furthermore, it ignores the similarities of the dependence of g_{true} and V_G on $[Tl^+]$ (Fig. 8, A and B), which seem to indicate that conduction and gating are coupled

as expected for processes of ion/channel interaction in the selectivity filter. Thus, the model suggested here employs two separate mechanisms for the exponential increase of R (Fig. 7) and the dependence of the characteristic parameters on [Tl^+] (Fig. 8).

(a) For the voltage dependence of gating, a model similar to that of Schroeder and Hansen (2007) is considered, but here with the assumption of luminal instead of cytosolic diffusion limitation. There may be two objections. (1) It may be argued that diffusion limitation at the sink side would limit the effect of exponential increase of the voltage-driven rate constant in the selectivity filter. Equations A4A and A4B in the Appendix show that it does not. Thus, a model relating fast gating to diffusion limitation on both sides is feasible. (2) Diffusion limitation at the luminal side is less obvious. It becomes prominent only when the negative charges at the pore mouth are neutralized by mutations in Kir2.1 (Alagem et al., 2001; Murata et al., 2002). Nevertheless, there is a small gating effect at negative potentials in WT of MaxiK as shown in Fig. 7 A. Below it is suggested that this small gating effect may be aggravated by the accumulation of Tl^+ in the cavity (according to a mechanism in Kir2.1 as proposed by Lu et al., 2001) or in the selectivity filter as discussed below.

Diffusion limitation at the luminal side may be caused by two different putative mechanisms that lead to saturation of I_{true} with increasing negative membrane potentials. The first mechanism causing the exponential increase in R_k (Fig. 7) starts from the assumption of diffusion limitation on the luminal side as corresponding to the cytosolic diffusion limitation assumed by Schroeder and Hansen (2007) for gating at positive potentials. The second alternative mechanism causes current saturation by the introduction of the law of transport site conservation as postulated in the Class I model of Hansen (Hansen et al., 1981; Hansen, 1986) or by the single-file model of Nelson (2002).

Ion depletion occurs at the outmost inner or outmost external ion binding site of the selectivity filter for outward or inward currents, respectively. This depletion is presented by the empty oxygen ring shown in the 1,3 or 2,4 position of the selectivity filter in KcsA in Fig. 6 of Morais-Cabral et al. (2001). The occupation of these sites (near the cavity for outward current or near the external vestibule for inward currents) decreases exponentially with the driving force. Similar to the model in Schroeder and Hansen (2007) we assume that the gating factor R increases with the inverse occupation of these sites.

The second model of diffusion limitation (availability of an empty site at the entrance) may also shed some new light on the model in Schroeder and Hansen (2007). There, one problem was mentioned, i.e., current reduction by cytosolic sugars (as suggested by the experiments on MaxiK by Brelidze and Magleby, 2005) did not influence fast gating in outward currents. However, if the ion depletion is caused by the second model and not solely by cytosolic diffusion limitation, then the sugar experiments need not to be a contradiction to the basic concept of the model of Schroeder and Hansen (2007).

(b) For the dependence of gating parameters on [Tl^+] (as described by g_{true}, V_G and $R_{k,0}$ in Fig. 8), modulatory sites have to be considered that modify the voltage-induced gating behavior in Fig. 7 in a parametric way. Indications that the gating mechanisms considered in the Appendix can be modulated by other sites, e.g., changes in backbone filter interactions came from spontaneous changes in gating behavior of MaxiK (Schroeder et al., 2004). A transition from a slow gating mode with $I_{app} = I_{true}$ to a fast gating mode with smaller I_{app} and back could be shown to be related to a spontaneous change in k_{OC}, i.e., in the lifetime of the open state (Schroeder and Hansen, 2006). k_{OC} was also the target of K^+ depletion (Schroeder and Hansen, 2007).

Candidates for these modulatory sites are Tl^+ binding sites at the luminal surface, the filter, or the cavity. Since there is no evidence for luminal Tl^+ binding sites, we concentrate the considerations on the selectivity filter and the cavity. We can assume that roughly the same mole fraction holds throughout the channel because I_{true} changes only by 40% for all mole fractions (Fig. 5 B and Fig. 8 A), thus Tl^+ enrichment in the cavity or the filter reflects the luminal mole fraction.

Lu et al. (2001) found that interaction of Tl^+ with C169 in the cavity of Kir2.1 induces structural changes that lead to the flickery state and subconductance levels (which can probably be shown to be related to the same mechanism if temporal resolution were high enough). In GIRK2, Bichet et al. (2006) found an influence of the cavity ion on the chance of another ion to leave the filter, thus influencing conductivity. Thus, changes in the ion concentration in the cavity can exert a parallel effect on V_G and on I_{true}.

The idea of destabilization of the selectivity filter by Tl^+ is even more established. Zhou and MacKinnon (2003) found that 20 mM K^+ is necessary to stabilize the open crystal structure of KcsA, whereas in the case of Tl^+ 80 mM was required. They found higher electron densities for Tl^+ than for K^+ in the filter sites. Furthermore, interaction of Tl^+ with the carbonyl groups in the filter destabilizes the open state and increases the unblocking rate for Ba^{2+} in Kir 2.1 (Lu et al., 2001).

Even though it is obvious that the gating events in the μs range are different from those in the ms range (Fig. 1 and Piskorowski and Aldrich, 2006), it cannot be denied that there is one peculiar common feature, i.e., the role of the Tl^+ concentrations around 50 mM. Piskorowski and Aldrich found that the dependence of the mean open time and the number of openings per bursts saturated around 50 mM Tl^+. Fig. 7 (A and B) shows the dependence on [Tl^+] of single-channel

conductivity (g_{true}) and of the characteristic voltage of gating (V_G). Saturation for both curves starts at ~50 mM Tl^+. The peculiar role of mole fractions with concentrations around 50 mM Tl^+ is also found by Piskorowski and Aldrich (2006) in the absolute values of the rate constant k_{OC}, i.e., the Tl^+-induced change in mean open times ($1/k_{OC}$ in the range of 1 to 2.5 ms) ended at these concentrations. At higher concentrations, mean open times stayed constant. This corresponds to the increase of k_{OC} up to 50 mM in Fig. 6 A and to the horizontal line at higher concentrations.

The above similarities may support the hypothesis of two different sites, one for the effect of ion depletion causing the exponential increase of the gating factor and the other one causing parametric changes of this gating. This support comes from the finding that Tl^+ influences the stability of the open state of µs gating and of ms gating in a similar way. A Tl^+-induced conformational change of the protein backbone may be expected to influence both fast and slow gating.

Nevertheless, the Tl^+-induced effects are different with respect to the mean closed time. Piskorowski and Aldrich (2006) have not found an effect on the mean closed time (~100 µs) and also in Fig. 1 B the effect is much smaller than that on open time (Fig. 1 A). In the case of µs gating, Fig. 6 A shows a decrease of k_{CO} at concentrations >50 mM. An analysis combining the results of fast and slow gating is expected from fitting the time series of the present investigation with the "Great Markov Model." However, reaching this goal may take some time. The SQ fit (subsequent HMM and β fit, Schroeder et al., 2005) is an adequate tool for gating analysis with a wide range of time constants, but the still unsolved problem is the finding of the correct Markov model. The O-O-C-C-C model used by Farokhi et al. (2000) and Hansen et al. (2003) for Tl^+-induced gating in the MaxiK-like channel in *Chara* failed when the β fit was employed to the full amplitude histogram. It had to be replaced by a C-O-C-C-O model with separate O states. This, however, is just the beginning of a long journey.

A final comment should deal with the nature of binding sites. It is probably not reasonable to assume some sort of covalent binding. Instead, a "site of interaction" should be postulated. This site feels the forces between ion and channel structure. Changes in these forces as caused by changes in ionic milieu (concentration and kind of ion) result in conformational changes of the protein. These conformational changes modify rate constants in a parametric way (Hansen et al., 2003). Such a model has several consequences. Due to the averaging effect of the deformations of the involved protein moieties, the time constants of the observed changes in gating are not related to the permeation times of single ions. Thus, the parametric effect on rate constants probably cannot be modeled by classical enzyme kinetics. Instead MD simulations are more adequate to estimate the effect of conformational changes on the rate constants of gating.

The last feature that has to be explained is that an effect of Tl^+ on fast gating (inducing a negative slope in I_{app}) is only observed in inward, but not in outward currents (Fig. 5 C). Outward currents lead to ion depletion in the cavity and/or the innermost sites of the filter (Schroeder and Hansen, 2007) in contrast to an accumulation by inward currents. This may attenuate the difference between the ion/channel interactions of Tl^+ and K^+.

The discussion of the models above shows that it is difficult to extract a unique model from the physiological data. Nevertheless, there is a clear message: the selectivity filter is a wobbly device whose stability depends on the proper ionic milieu. This implies that a great portion of flexibility is required when the "snug fit" hypothesis is employed to explain the transport mechanism of the selectivity filter.

APPENDIX

If fast gating is influenced by changes in ion concentrations or by the occupation of putative sites, then the effects have to be considered that determine the current through the channel. There are two different mechanisms that alone or together can result in saturating IV curves as found in Fig. 5 B: a linear or a cyclic reaction scheme. It has to be mentioned that rate limitation by the loading reaction is already involved when the IV curve increases linearly instead of exponentially with membrane potential. Saturation in its common meaning (i.e., horizontal asymptotes) occurs only at very high positive potentials in Fig. 5 B.

A. A Linear Scheme Consisting of Four Compartments: Cytosol (P), Cavity (S), External Vestibule (E), Lumen (L) According to Fig. 8 in Schroeder and Hansen (2007)

The gross reaction constants k_{PL} and k_{LP} of transfer of one ion from one side of the membrane to the other side are proportional to the entering reactions k_{PS} or k_{LE}, respectively; since they do not occur in the denominator. (In Eq. A1, arrows from A to B present the rate constant k_{AB}. Arrows in a row are multiplied, and the products of the rows are added, Sanders and Hansen, 1981).

$$k_{PL} = \frac{\begin{array}{cccc} \rightarrow & \rightarrow & \rightarrow & \\ P & S & E & L \\ & \rightarrow & \rightarrow & \\ \leftarrow & & \rightarrow & \\ \leftarrow & \leftarrow & & \end{array}}{} \approx k_{PS} \qquad k_{LP} = \frac{\begin{array}{cccc} \leftarrow & \leftarrow & \leftarrow & \\ P & S & E & L \\ & \rightarrow & \rightarrow & \\ \leftarrow & & \rightarrow & \\ \leftarrow & \leftarrow & & \end{array}}{} \approx k_{LE} \tag{A1a,b}$$

The last righthand expressions in Eqs. A1a,b are obtained for high positive or high negative membrane potentials when the voltage-driven k_{SE} or k_{ES} become

very great, respectively. Because of Eq. A1,a,b, the entering rate constants determine the saturation of I_{true} (Fig. 5).

The depletion of the intermediate compartments S or E with increasing k_{SE} or k_{ES}, respectively, is obtained from the balance of influx and efflux (ignoring back flow through the filter).

$$[S] = \frac{k_{PS}}{k_{SP} + k_{SL}}[P] \qquad [E] = \frac{k_{LE}}{k_{EL} + k_{EP}}[L] \tag{A2a,b}$$

The rate constants k_{SE} and k_{ES} being part of k_{SL} and k_{EP}, respectively, are voltage dependent (s = fraction of the membrane voltage that drops over the filter).

$$k_{SE} = k_{SE,0} \exp\left(\frac{esV}{kT}\right) \qquad k_{ES} = k_{ES,0} \exp\left(\frac{-esV}{kT}\right) \tag{A3a,b}$$

For the ion depletion in the intermediate compartments S or E, it is important that the exit rate constants k_{EL} or k_{SP} do not limit the exponential increase of the voltage-sensitive rate constants k_{SE} or k_{ES}, respectively.

$$k_{SL} = \overrightarrow{\overrightarrow{S\ E\ L}} \approx k_{SE} \qquad k_{EP} = \overleftarrow{\overleftarrow{P\ S\ E}} \approx k_{ES} \tag{A4a,b}$$

Thus, depletion by diffusion limitation can work for either direction of the current. It may be different for outward and inward currents depending on the rate constants k_{PS} and k_{LE} in Eqs. A2a,b, respectively.

For [Tl^+] up to 50 mM, it is assumed that the lifetime of the open state $1/k_{OC}$ is proportional to the occupation [E] and that k_{CO} is constant, according to Schroeder and Hansen (2007). Inserting Eqs. A3b and 4b into Eq. A2b and $k_{OC} = 1/[E]$ into Eq. 4a leads to the exponential dependence of the gating factor R in Eq. 5. At [Tl^+] > 50 mM, it has to be assumed that k_{CO} is proportional to [E] in order to account for the results in Fig. 6 (A and B).

B. Introduction of the Law of Site Conservation for the Selectivity Filter

In cyclic reaction schemes like the Class I model of Hansen et al. (1981) or the single-file model of Nelson (2002), another effect causes saturation, namely the law of transport site conservation. In both models, the sum of configurations with empty sites on the luminal and cytosolic site (plus with all sites occupied, Nelson, 2002) is constant, e.g., "1" in single-channel experiments. However, the ratio of open sites (ready to accept an ion) close to the external vestibule (Θ_E) to those close to the cavity (Θ_C) is

$$\frac{\Theta_E}{\Theta_C} = \exp\left(\frac{e_o sV}{kT}\right), \tag{A5}$$

with s being the electrical distance, V the membrane potential, and e_0, k, and T having their usual meaning.

Since enrichment on one side cannot exceed Θ_C or $\Theta_E = 1$, the occupation at the other side has to decrease exponentially with V, i.e., Θ_C for outward currents and Θ_E for inward currents.

In terms of the scheme of site occupation as suggested for KcsA by Morais-Cabral et al. (2001), the transport cycle for outward currents would be as follows. State 2,4 with empty outer oxygen ring sits there and waits for a K^+ ion to jump into the filter. After the jump, all three K^+ ions move in a concerted single-file action, and one K^+ ion exits at the cavity side, leaving the channel in the 1,3 configuration. The 1,3 configuration is converted to the 2,4 configuration via an intermediate state with the ion and the water in the plane of the oxygen rings. At negative potentials, the ratio of the lifetime of 1,3 configuration (Θ_E) to that of the 2,4 configuration (Θ_C) is given by Eq. A5 (ignoring the other two states that may be suitably included in Θ_E or Θ_C). Thus, the occupation of the outer oxygen ring by an ion decreases exponentially with negative membrane potential. This would create the behavior in Fig. 6 if we assume that the lifetime of the open state τ_O is proportional to the average lifetime of the occupation of the configurations with a K^+ in (or near) the outer oxygen ring. This holds for concentrations <50 mM Tl^+

$$\frac{1}{k_{OC}} = \tau_O = c_1(\overline{[conf\,1,3]}), \tag{A6a}$$

with [$conf$ 1,3] being the average lifetime of the 1,3 configuration.

Above this concentration, the lifetime of the closed state τ_C would be lengthened.

$$\frac{1}{\tau_C} = k_{CO} = c_2(\overline{[conf\,1,3]}). \tag{A6b}$$

Insertion of Eq. A6a,b into Eq. 4a leads to the exponential dependence of the gating factor R (Eq. 5) similar to the calculations of Schroeder and Hansen (2007).

We are grateful to Imke Diddens for doing some of the patch clamp experiments and to Sonja Vollbehr for taking care of the HEK cells. The cells were a gift from Prof. U. Seydel and Dr. A. Schromm, Research Center, Borstel.

This work was supported by the Deutsche Forschungsgemeinschaft Ha712/14-1,2.

Olaf S. Andersen served as editor.

Submitted: 4 January 2008
Accepted: 5 March 2008

REFERENCES

Alagem, N., M. Dvir, and E. Reveny. 2001. Mechanism of Ba^{2+} block of a mouse inwardly rectifying K^+ channel: differential contribution by two discrete residues. *J. Physiol.* 534:381–393.

Bernèche, S., and B. Roux. 2000. Molecular dynamics of the KcsA K^+ channel in a bilayer membrane. *Biophys. J.* 78:2900–2917.

Bernèche, S., and B. Roux. 2005. A gate in the selectivity filter of potassium channels. *Structure.* 13:591–600.

Bezanilla, F., and C.M. Armstrong. 1972. Negative conductance caused by the entry of sodium and cesium ions into the K channels of squid axon. *J. Gen. Physiol.* 60:588–608.

Bichet, D., M. Grabe, Y.N. Jan, and L.Y. Jan. 2006. Electrostatic interactions in the channel cavity as an important determinant of potassium channel selectivity. *Proc. Natl. Acad. Sci. USA.* 103:14355–14360.

Blatz, A.L., and K.L. Magleby. 1984. Ion conductance and selectivity of single calcium-activated potassium channels in cultured rat muscle. *J. Gen. Physiol.* 84:1–23.

Blunck, R., J.F. Cordero-Morales, L.G. Cuello, E. Perozo, and F. Bezanilla. 2006. Detection of the opening of the bundle crossing in KcsA with fluorescence lifetime spectroscopy reveals the existence of two gates for ion conduction. *J. Gen. Physiol.* 128:569–581.

Brelidze, T.I., and K.L. Magleby. 2005. Probing the geometry of the inner vestibule of BK channels with sugars. *J. Gen. Physiol.* 126:105–121.

Caceci, M.S., and W.P. Cacheris. 1984. Fitting curves to data-the simplex algorithm is the answer. *BYTE.* 5/84:340–362.

Capener, C.E., P. Proks, F.M. Ashcroft, and M.P.S. Sansom. 2003. Filter flexibility in a mammalian K channel: models and simulations of Kir6.2 mutants. *Biophys. J.* 84:2345–2356.

Claydon, T.W., S.Y. Makary, K.M. Dibb, and M.R. Boyett. 2003. The selectivity filter may act as the agonist-activated gate in the G protein-activated Kir3.1/Kir3.4 K^+ channel. *J. Biol. Chem.* 278:50654–50663.

Choi, K.L., R.W. Aldrich, and G. Yellen. 1991. Tetraethylammonium blockade distinguishes two inactivation mechanisms in voltage-gated K^+ channels. *Proc. Natl. Acad. Sci. USA.* 88:5092–5095.

Doyle, D.A., J. Morais-Cabral, R.A. Pfuetzner, A. Kuo, J.M. Gulbis, S.L. Cohen, B.T. Chait, and R. MacKinnon. 1998. The structure of the potassium channel: molecular basis of K^+ conduction and selectivity. *Science.* 280:69–77.

Draber, S., and U.P. Hansen. 1994. Fast single-channel measurements resolve the blocking effect of Cs^+ on the K^+ channel. *Biophys. J.* 67:120–129.

Eisenman, G. 1962. Cation selective electrodes and their mode of operation. *Biophys. J.* 2:259–323.

Eisenman, G., and R. Horn. 1983. Ion selectivity revisited: the role of kinetic and equilibrium processes in ion permeation through channels. *J. Membr. Biol.* 76:197–225.

Farokhi, A., M. Keunecke, and U.P. Hansen. 2000. The anomalous mole fraction effect in *Chara*: gating at the edge of temporal resolution. *Biophys. J.* 79:3072–3082.

FitzHugh, R. 1983. Statistical properties of the asymmetric random telegraph signal with application to single-channel analysis. *Math. Biosci.* 64:75–89.

Gazzarrini, S., J.L. Van Etten, D. DiFrancesco, G. Thiel, and A. Moroni. 2002. Voltage-dependence of virus-encoded miniature K^+ channel Kcv. *J. Membr. Biol.* 187:15–25.

Gazzarrini, S., A. Abenavoli, D. Gradmann, G. Thiel, and A. Moroni. 2006. Electrokinetics of miniature K^+ channel: open-state *V* sensitivity and inhibition by K^+ driving force. *J. Membr. Biol.* 214:9–17.

Gibor, G., D. Yakubovich, A. Rosenhouse-Dantsker, A. Peretz, H. Schottelndreier, G. Seebohm, N. Dascal, D.E. Logothetis, Y. Paas, and B. Attali. 2007. An inactivation gate in the selectivity filter of KCNQ1 potassium channels. *Biophys. J.* 93:4159–4172.

Hansen, U.P. 1986. Reaction kinetic models of pumps, cotransporters and channels. *In* Ion Channels and Electrogenic Pumps in Biomembranes. Abstracts of Lectures and Posters. Osaka University, Osaka, Japan. L13–L33.

Hansen, U.P., D. Gradmann, D. Sanders, and C.L. Slayman. 1981. Interpretation of current-voltage relationships for "active" ion transport systems: I. Steady-state reaction-kinetic analysis of class-I mechanisms. *J. Membr. Biol.* 63:165–190.

Hansen, U.P., O. Cakan, M. Abshagen, and A. Farokhi. 2003. Gating models of the anomalous mole fraction effect of single-channel current in *Chara*. *J. Membr. Biol.* 192:45–63.

Harlfinger, P. 2003. Detection of Fast Rate Constants in Markov Processes by Means of a Joint Evaluation of Amplitude Histograms and Temporal Behavior. PhD thesis. University of Kiel, Kiel, Germany. www.zbm.uni-kiel.de/lehre/diss.html

Huth, T. 2005. 4-Mode-Gating-Model: Modeling the Inactivation of the Sodium Channel. PhD thesis. University of Kiel, Kiel, Germany. www.zbm.uni-kiel.de/lehre/diss.html

Immke, D., M. Wood, L. Kiss, and S.J. Korn. 1999. Potassium-dependent changes in the conformation of the Kv2.1 potassium channel pore. *J. Gen. Physiol.* 113:819–836.

Ilan, N., and S.A.N. Goldstein. 2001. KCNKØ: single, cloned potassium leak channels are multi-ion pores. *Biophys. J.* 80:241–253.

Kang, M., A. Moroni, S. Gazzarrini, D. DiFrancesco, G. Thiel, M. Severino, and J.L. Van Etten. 2004. Small potassium ion channel proteins encoded by *Chlorella* viruses. *Proc. Natl. Acad. Sci. USA.* 101:5318–5324.

Kawahara, K., M. Hunter, and G. Giebisch. 1990. Calcium-activated potassium channels in the luminal membrane of *Amphiuma* diluting segment: voltage-dependent block by intracellular Na^+ upon depolarization. *Pflugers Arch.* 416:422–427.

Kurata, H.T., and D. Fedida. 2006. A structural interpretation of voltage-gated potassium channel inactivation. *Prog. Biophys. Mol. Biol.* 92:185–208.

Kiss, L., J. LoTurco, and S.J. Korn. 1999. Contribution of the selectivity filter to inactivation in potassium channels. *Biophys. J.* 76:253–263.

Klieber, H.-G., and D. Gradmann. 1993. Enzyme kinetics of the prime K^+ channel in the tonoplast of *Chara*: selectivity and inhibition. *J. Membr. Biol.* 132:253–265.

Larsson, H.P., and F. Elinder. 2000. A conserved glutamate is important for slow inactivation in K^+ channels. *Neuron.* 27:573–583.

LeMasurier, M., L. Heginbotham, and C. Miller. 2001. KcsA: it's a potassium channel. *J. Gen. Physiol.* 118:303–318.

Loots, E., and E.Y. Isacoff. 2000. Molecular coupling of S4 to a K^+ channel's slow inactivation gate. *J. Gen. Physiol.* 116:623–635.

Lopez-Barneo, J., T. Hoshi, S.H. Heinemann, and R.W. Aldrich. 1993. Effects of external cations and mutations in the pore region on C-type inactivation of *Shaker* potassium channels. *Receptors Channels.* 1:61–71.

Lu, R., A. Alioua, Y. Kumar, M. Eghbali, E. Stefani, and L. Toro. 2006. MaxiK channel partners: physiological impact. *J. Physiol.* 570:65–72.

Lu, T., L. Wu, J. Xiao, and J. Yang. 2001. Permeant-ion dependent changes in gating of Kir2.1 inward rectifier potassium channels. *J. Gen. Physiol.* 118:509–521.

Morais-Cabral, J.H., Y. Zhou, and R. MacKinnon. 2001. Energetic optimization of ion conduction rate by the K^+ selectivity filter. *Nature.* 414:37–42.

Mullins, L.J. 1959. The penetration of some cations into muscle. *J. Gen. Physiol.* 42:817–829.

Murata, Y., Y. Fujiwara, and Y. Kubo. 2002. Identification of a site involved in the block by extracellular Mg^{2+} and Ba^{2+} as well as permeation of K^+ in the Kir2.1 K^+ channel. *J. Physiol.* 544:665–677.

Nimigean, C.M., and C. Miller. 2002. Na^+ block and permeation in a K^+ channel of known structure. *J. Gen. Physiol.* 120:323–335.

Nelson, P.H. 2002. A permeation theory for single-file ion channels: corresponding occupancy states produce Michaelis-Menton behaviour. *J. Chem. Phys.* 117:11396–11403.

Noskov, S.Y., and B. Roux. 2006. Ion selectivity in potassium channels. *Biophys. Chem.* 124:279–291.

Noskov, S.Y., and B. Roux. 2007. Importance of hydration and dynamics on the selectivity of the KcsA and NaK channels. *J. Gen. Physiol.* 129:135–143.

Noskov, S.Y., S. Bernèche, and B. Roux. 2004. Control of ion selectivity in potassium channels by electrostatic and dynamic properties of carbonyl ligands. *Nature.* 431:830–834.

Piskorowski, R.A., and R.W. Aldrich. 2006. Relationship between pore occupancy and gating in BK potassium channels. *J. Gen. Physiol.* 127:557–576.

Proks, P., C.E. Capener, P. Jones, and F.M. Ashcroft. 2001. Mutations within the P-loop of Kir6.2 modulate the intraburst kinetics of the ATP-sensitive potassium channel. *J. Gen. Physiol.* 118:341–353.

Renart, M.L., F.N. Barrera, M.L. Molina, J.A. Encinar, J.A. Poveda, A.M. Fernandez, J. Gomez, and J.M. Gonzalez-Ros. 2006. Effects of conducting and blocking ions on the structure and stability of the potassium channel KcsA. *J. Biol. Chem.* 281:29905–29915.

Riessner, T. 1998. Level Detection and Extended Beta Distributions for the Analysis of Fast Rate Constants of Markov Processes in Sampled Data. Shaker-Verlag, Aachen, Germany. 74 pp.

Riessner, T., F. Woelk, M. Abshagen-Keunecke, A. Caliebe, and U.P. Hansen. 2002. A new level detector for ion channel analysis. *J. Membr. Biol.* 189:105–118.

Sanders, D., and U.P. Hansen. 1981. Mechanism of Cl^- transport at the plasma membrane of *Chara corallina*: II. Transinhibition and the determination of H^+/Cl^- binding order from a reaction kinetic model. *J. Membr. Biol.* 58:139–153.

Schroeder, I., and U.P. Hansen. 2006. Strengths and limits of beta distributions as a means of reconstructing the true single-channel current in patch clamp time series with fast gating. *J. Membr. Biol.* 210:199–212.

Schroeder, I., and U.P. Hansen. 2007. Saturation and μs-gating of current indicate depletion-induced instability of the MaxiK selectivity filter. *J. Gen. Physiol.* 130:83–97.

Schroeder, I., T. Huth, V. Suitchmezian, J. Jarosik, S. Schnell, and U.P. Hansen. 2004. Distributions-per-level: a means of testing level detectors and models of patch clamp data. *J. Membr. Biol.* 197:49–58.

Schroeder, I., P. Harlfinger, T. Huth, and U.P. Hansen. 2005. A subsequent fit of time series and amplitude histogram of patch clamp data reveals rate-constants up to 1 μs^{-1}. *J. Membr. Biol.* 203:83–99.

Schultze, R., and S. Draber. 1993. A nonlinear filter algorithm for detection of jumps in patch-clamp data. *J. Membr. Biol.* 132:41–52.

Shim, J.W., M. Yang, and L.-Q. Gu. 2007. In vitro synthesis, tetramerization and single channel characterization of virus-encoded potassium channel Kcv. *FEBS Lett.* 581:1027–1034.

Starkus, J.G., L. Kuschel, M.D. Rayner, and S.H. Heinemann. 1997. Ion conduction through C-type inactivated *Shaker* channels. *J. Gen. Physiol.* 110:539–550.

Varma, S., and S.B. Rempe. 2007. Tuning ion coordination architectures to enable selective partitioning. *Biophys. J.* 93:1093–1109.

Weise, R., and D. Gradmann. 2000. Effects of Na^+ on the predominant K^+ channel in the tonoplast of *Chara*: decrease of conductance by blocks in 100 ns range and induction of oligo- or poly-subconductance gating modes. *J. Membr. Biol.* 175:87–93.

Xie, L.H., S.A. John, B. Ribalet, and J.N. Weiss. 2004. Regulation of gating by negative charges in the cytoplasmic pore in the Kir2.1 channel. *J. Physiol.* 561(1):159–168.

Yellen, G. 1998. The moving parts of voltage-gated ion channels. *Q. Rev. Biophys.* 31:239–295.

Yi, B.A., Y.-F. Lin, Y.N. Jan, and L.Y. Jan. 2001. Yeast screen for constitutively active mutant G protein–activated potassium channels. *Neuron.* 29:657–667.

Zheng, J., and F.J. Sigworth. 1998. Intermediate conductance during deactivation of heteromultimeric *Shaker* potassium channels. *J. Gen. Physiol.* 112:457–474.

Zheng, J., L. Venkataramanan, and F.J. Sigworth. 2001. Hidden Markov model analysis of intermediate gating steps associated with the pore gate of *Shaker* potassium channels. *J. Gen. Physiol.* 118:547–562.

Zhou, Y., and R. MacKinnon. 2003. The occupancy of ions in the K^+ selectivity filter: Charge balance and coupling of ion binding to a protein conformational change underlie high conduction rates. *J. Mol. Biol.* 333:965–975.

Zhou, Y., and R. MacKinnon. 2004. Ion binding affinity in the cavity of the KcsA potassium channel. *Biochemistry.* 43:4978–4982.